# High Damped Digital Current Controller based on Active Resistance for AC Machines

Xin Yuan, *Senior Member, IEEE*, Junkai Wen, Shuangxia Niu, *Senior Member, IEEE*, and Mingjin Hu

***Abstract*—Due to the simple structure and good disturbance rejection, the proportional-integral (PI) digital current controller with active resistance term feedback (ARTF) has been widely utilized in high-performance AC motor drives such as EV powertrain. However, the complexity of discrete-time AC machine model, current performance degradation of the PI controller at high bandwidth condition, and ARTF digital delay effect lead to the difficulty of design and tuning of the controller. To address these issues, without employing current prediction mechanism, a novel high damped digital current controller with ARTF is proposed in this paper, which can achieve deadbeat dynamic response performance, possess strong disturbance rejection with no overshoot in theory, suppress the ARTF digital delay issue effectively, and own lower parameter sensitivity. The effectiveness of the proposed controller is fully validated through a practical AC machine drive test rig.**

***Index Terms*—Active resistance term feedback, digital controller, deadbeat response, EV powertrain, PI current control.**

## NOMENCLATURE

| | |
|---|---|
| $U_{dq}$ | dq-axis stator voltages |
| $i_{dq}$ | dq-axis stator currents |
| $i_{dq}^{ref}$ | Reference dq-axis stator currents |
| $\omega_e$ | Electrical angular speed |
| $T_s$ | System sampling and control period |
| $L_d$ | Actual d-axis stator inductance |
| $L_q$ | Actual q-axis stator inductance |
| $R_s$ | Actual stator resistance |
| $e_{dq}$ | Actual dq-axis back-emf voltages |
| $D_{dq}$ | dq-axis voltage disturbances |
| $\psi_f$ | Actual dq-axis flux linkage |
| $L_{dC}$ | Nominal d-axis inductance in controller |
| $L_{qC}$ | Nominal q-axis inductance in controller |
| $R_C$ | Nominal stator resistance in controller |
| $\psi_{fC}$ | Nominal dq-axis flux linkage in controller |
| $U_{dq}^{ref}$ | Reference dq-axis stator voltages |

## I. Introduction

### A. Classical PI control with internal model control

In order to realize excellent machine torque performance, current control methodologies have been developed in AC machine drives to achieve high dynamic performance, good disturbance rejection and strong parameter robustness [1]. Due to the fast dynamic response, the predictive current control methods have been getting wide attention within ten years [2]. However, the conventional predictive current control method is strongly sensitive to the disturbance caused by the parameter mismatch [3]. Due to the low calculation burden and good parameter robustness, the PI current control method is most commonly used in industrial applications. The PI coefficients can be easily designed based on the internal model control (IMC) principle [4], but axis-cross coupling terms will degrade the PI current control performance. In this case, a state feedback decoupling PI current controller was proposed, where the imaginary part of the plant pole can be fully canceled by the feedback variables [5]. In order to lower the sensitivity to the parameter mismatch, the complex vector PI current controller was developed, where a decoupling item that varies with the speed is added to realize the dq-axis decoupling [6]. However, the disturbance rejection ability of the PI controller is insufficient due to low stiffness and damping characteristics of the plant [7], [8].

### B. Delay issue in digital system for AC machines

Previously, these classical current control [4]–[6] were designed based on the continuous-time model of AC machines. However, with rapid growing development of digital systems such as ARM, DSP, and FPGA microprocessors, the overall current performance will deteriorate with the designed continuous-time model framework in digital systems when the current regulator is tuned for high bandwidth or the operating condition is under high fundamental excitation frequencies relative to the sampling frequencies. The continuous-time methods can be discretized by using approximated discretization methods such as Euler approximation and Tustin approximation, but it can cause AC machine parameter mismatch with IMC principle [9]. Furthermore, the computation delay and modulation delay caused by PWM were not considered. To ease the negative impact, an exact zero-order hold (ZOH) equivalent discrete PMSMs model considering the computation and modulation delay has been developed and attracted widespread attention [10]. However, due to the existence of the calculation of the matrix exponential, the exact model is complicated, and its order is unnecessarily high. Therefore, many methods focused on the model simplification were developed

Junkai Wen, Shuangxia Niu, and Mingjin Hu are with the Department of Electrical and Electronic Engineering, The Hong Kong Polytechnic University, Hong Kong 999077, China (e-mail: 22116996r@connect.polyu.hk; eesxniu@polyu. edu.hk; mingjin.hu@polyu.edu.hk).

Xin Yuan is with the School of Engineering, University of Aberdeen, AB24 3UF Aberdeen, U.K. (e-mail: xin.yuan@abdn.ac.uk).

[11], [12]. Hinkkanen et al. applied the series expansion of the matrix exponential to simplify the model [11], and Hu et al. [12] proposed a simplified model for salient machines by utilizing the series expansion to reduce the calculation.

In general, the approaches for improving the disturbance rejection are are dividied into two main items, i. e., disturbance observers [7] and active resistance term feedback (ARTF). The design and complexity of the ARTF is much simpler than that of the former method. The ARTF method was first developed in the continuous-time model, and widely used in the design of current and speed controllers [13]. However, it has been found that the computation and modulation delay has a negative effect on the ARTF structure, and as the strength of the ARTF increases, the easier poles approach the unit circle' boundary, resulting in low damping and the current oscillation [14], [15].

A two-degree-of-freedom digital PI current control was proposed, where the optimum value for active resistance was derived to optimize the setting time and overshoot [14]. Vukosavic et al. proposed a digital current controller with an error-free sampling scheme based on the ARTF, where a delay model is added into the current control structure and it improved the disturbance rejection by extending the range of permissible value of the active resistance [16]. In addition, the prediction scheme was employed to suppress the ARTF delay effect [17]. In order to further improve the dynamic performance, an improved digital current controller with a digital IMC current estimator was proposed, where the predicted current is utilized as the ARTF delay compensation and feedback of the current controller simultaneously [18].

### C. Motivation and Innovation

Motivated by these facts, abandoning the employment of the current prediction, this paper proposes a novel framework of digital current controller with ARTF, where deadbeat dynamic response performance, strong disturbance rejection with no overshoot in theory, and lower parameter sensitivity can be achieved. The main innovations and contributions of this work can be listed as follows: 1) Different from the PI current controllers based on IMC methods, i.e., [13], [16], [17] that the system will occur the overshoot with high value of bandwidth, a novel framework of the digital current controller can improve the dynamic response performance and achieve deadbeat response, where the closed-loop transfer function can still be a first-order system and it can achieve high dynamic response performance, and parameter robustness performance. 2) Without employing any current prediction mechanism, i.e., [17], [18], a high-damped framework is first proposed to to suppress the negative impact of the ARTF delay on system and the current response performance are analysed in detailed. The proposed framework can extend the range of permissible value of the active resistance without compromising stability and reduce the current oscillation caused by the ARTF delay. 3) To optimize the digital implementation and perform anti-windup control, a proportional-integral-inertia (PIN) framework is proposed in detail and the computational burden becomes low.

TABLE I
RELATIONSHIP BETWEEN $\theta_e$ AND $U_a^{'}, U_b^{'}, U_c^{'}$

| Region | $\theta_e$ | The value of $U_a^{'}$, $U_b^{'}$, $U_c^{'}$ |
|---|---|---|
| I | $-\frac{\pi}{6} \rightarrow \frac{\pi}{6}$ | $\frac{4\lvert U\rvert}{3}, -\frac{2\lvert U\rvert}{3}, -\frac{2\lvert U\rvert}{3}$ |
| II | $\frac{\pi}{6} \rightarrow \frac{3\pi}{6}$ | $\frac{2\lvert U\rvert}{3}, \frac{2\lvert U\rvert}{3}, -\frac{4\lvert U\rvert}{3}$ |
| III | $\frac{3\pi}{6} \rightarrow \frac{5\pi}{6}$ | $-\frac{2\lvert U\rvert}{3}, \frac{2\lvert U\rvert}{3}, -\frac{2\lvert U\rvert}{3}$ |
| IV | $\frac{5\pi}{6} \rightarrow \frac{7\pi}{6}$ | $-\frac{4\lvert U\rvert}{3}, \frac{2\lvert U\rvert}{3}, \frac{2\lvert U\rvert}{3}$ |
| V | $\frac{7\pi}{6} \rightarrow \frac{9\pi}{6}$ | $-\frac{2\lvert U\rvert}{3}, -\frac{2\lvert U\rvert}{3}, \frac{4\lvert U\rvert}{3}$ |
| VI | $\frac{9\pi}{6} \rightarrow \frac{11\pi}{6}$ | $\frac{2\lvert U\rvert}{3}, -\frac{4\lvert U\rvert}{3}, \frac{2\lvert U\rvert}{3}$ |

### D. Paper Organization

This paper is organized as follows. Sections II presents continuous-time and an exact ZOH equivalent discrete-time AC machines models. The proposed deadbeat current controller framework is described in Section III. In Sections IV, four classical current control algorithms are compared in AC machine drive test rig. Finally, Section V concludes this paper. '

## II. Exact ZOH equivalent discrete-time AC machines model

### A. Continuous-time modeling for AC machines

In order to obtain excellent machine torque performance, an inverter nonlinearity should be compensated such as classical look-up-table (LUT) solution: The three-phase distorted voltages $U_a^{'}, U_b^{'}, U_c^{'}$ caused by inverter nonlinearity can be derived as follows [19], [20]:

$$\begin{cases} U_a^{'} = \frac{|U|}{3}\left[2tanh\left(i_a\right) - tanh\left(i_b\right) - tanh\left(i_c\right)\right] \\ U_b^{'} = \frac{|U|}{3}\left[2tanh\left(i_b\right) - tanh\left(i_a\right) - tanh\left(i_c\right)\right] \\ U_c^{'} = \frac{|U|}{3}\left[2tanh\left(i_c\right) - tanh\left(i_a\right) - tanh\left(i_b\right)\right] \end{cases} \quad (1)$$

where $i_a, i_b, i_c$ are A, B and C phase stator currents, respectively. $V_{dc}$ is the dc bus voltage. $tanh$ is the hyperbolic tangent function as same as arctan function [21]. The distorted voltage $|U|$ caused by the inverter nonlinearity can be compensated based on self-commissioning scheme [22]. The dq-axis distorted voltages matrix $U_{dq}^{'}$ can be obtained based on Clarke and Park transform of $U_a^{'}, U_b^{'}, U_c^{'}$. Since the position of the current vector is 90 degrees ahead of the AC machine electrical angle $\theta_e$, the relationship between $\theta_e$ and distorted voltages $U_a^{'}, U_b^{'}, U_c^{'}$ can be presented in Table I. After compensating for the inverter nonlinearity, the ideal continuous-time model of AC machines in synchronous frame can be presented as follows [7]:

$$U_{dq} = \boldsymbol{L}\dot{i}_{dq} + \boldsymbol{R}i_{dq} + \boldsymbol{C} + e_{dq} \quad (2)$$

where $\boldsymbol{L} = \begin{bmatrix} L_d & 0 \\ 0 & L_q \end{bmatrix}$, $\boldsymbol{R} = \begin{bmatrix} R_s & 0 \\ 0 & R_s \end{bmatrix}$, $\boldsymbol{C} = \begin{bmatrix} -\omega_e L_q i_q \\ \omega_e L_d i_d \end{bmatrix}$, $U_{dq} = \begin{bmatrix} U_d \\ U_q \end{bmatrix}$, $i_{dq} = \begin{bmatrix} i_d \\ i_q \end{bmatrix}$. It should be noted that $R_s$ stands for the estimation of the whole series resistance (motor and inverter). Decoupling of $\boldsymbol{C} + e_{dq}$ allows synchronous or

asynchronous machines to be modeled by using a resistor-inductor (RL) load model, and if $\boldsymbol{C}$ is not decoupled, it will be added in the AC machines model.

### B. Delay issue in digital system and exact ZOH equivalent discrete-time AC machines model

In order to provide sufficient t ime f or t he e xecution of control method in digital systems, the PWM reference updating is normally delayed , and this produces an execution delay [10]. Neglecting the oversampling techniques, there are generally four PWM updating and current sampling schemes, namely, symmetrical PWM with sampling at the start each carrier period (SPWMS), asymmetrical PWM with sampling at the start and in the middle of each carrier period (APWMD), symmetrical PWM with sampling in the middle of each carrier period (SPWMM), and asymmetrical PWM with sampling at the start each carrier period (APWMS). The execution delay time varies with different PWM updating and current sampling patterns, i.e., the execution delay is one $1T_s$ delay for SPWMS and APWMD, and $0.5T_s$ execution delay for SPWMM and APWMS. To simplify the digital system, the SPWMS is employed in this paper. It should be noted that the proposed current control universal for other PWM updating and current sampling schemes. Considering $e_{dq}$ as a load disturbance, the transfer function of exact ZOH equivalent discrete-time AC machines model $G_{p0}(z)$ can be expressed as follows [12]:

$$\begin{aligned} G_{p0}(z) =& \frac{i_{dq}(z)}{U_{dq}(z)} = \frac{\boldsymbol{\Delta}}{z(z\boldsymbol{I}-\boldsymbol{\Gamma})} \\ \Delta =& \boldsymbol{L}^{-1}\int_0^{T_s} e^{-\left(\frac{\boldsymbol{R}}{\boldsymbol{L}}+\boldsymbol{J}\omega_e\right)\tau} e^{\boldsymbol{J}\omega_e\tau} d\tau e^{-2\boldsymbol{J}\omega_e T_s} \\ \Gamma =& \boldsymbol{L}^{-1} e^{-\left(\frac{\boldsymbol{R}}{\boldsymbol{L}}+\boldsymbol{J}\omega_e\right)T_s}\boldsymbol{L} \end{aligned} \tag{3}$$

where $\boldsymbol{I}$ is the identity matrix, i.e., $\boldsymbol{I} = \begin{bmatrix}1 & 0\\ 0 & 1\end{bmatrix}$, $\boldsymbol{J} = \begin{bmatrix}0 & -1\\ 1 & 0\end{bmatrix}$, the matrix exponential $e^{\boldsymbol{J}x} = \begin{bmatrix}\cos x & -\sin x\\ \sin x & \cos x\end{bmatrix}$.

## III. Proposed deadbeat current controller framework

### A. ZOH equivalent discrete-time model with ARTF simplification

The exact ZOH equivalent discrete-time model is built, and the computational delay is taken into account. However, it can be seen from (3) that the exact discrete-time model involves the calculation of the exponential matrix, which is complicated and has the unnecessarily high order [11]. As a results, it leads some difficulty to the design of the controller and is not suitable for low cost practical system due to the large calculation burden. Hence, it is necessary to build a simplified model with series expansion of the matrix exponential (3):

$$e^{AT_s} = I + AT_s + \frac{A^2}{2!}T_s^2 + \cdots \frac{A^n}{n!}T_s^n \tag{4}$$

where n represents the order number of the series expansion of matrix exponential. In this paper, $n = 1$ is adopted. The transfer function of $G_{p1}(z)$ can be expressed as follows:

$$\begin{aligned} G_{p1}(z) =& \frac{i_{dq}(z)}{U_{dq}(z)} = \frac{\boldsymbol{\Delta}}{z(z\boldsymbol{I}-\boldsymbol{\Gamma})} \\ \boldsymbol{\Delta} =& \boldsymbol{L}^{-1}\int_0^{T_s} e^{-\left(\frac{\boldsymbol{R}}{\boldsymbol{L}}+\boldsymbol{J}\omega_e\right)\tau} e^{\boldsymbol{J}\omega_e\tau} d\tau e^{-2\boldsymbol{J}\omega_e T_s} \\ =& \begin{bmatrix}\frac{T_s}{L_d} & 0\\ 0 & \frac{T_s}{L_q}\end{bmatrix} e^{-2\boldsymbol{J}\omega_e T_s} \\ \boldsymbol{\Gamma} =& \boldsymbol{L}^{-1} e^{-\left(\frac{\boldsymbol{R}}{\boldsymbol{L}}+J\omega_e\right)T_s}\boldsymbol{L} = \begin{bmatrix}1-\frac{R_s}{L_d}T_s & \frac{L_q}{L_d}T_s\omega_e\\ -\frac{L_d}{L_q}T_s\omega_e & 1-\frac{R_s}{L_q}T_s\end{bmatrix} \end{aligned} \tag{5}$$

Due to the low stiffness and damping characteristics of the plant, the active resistance term feedback (ARTF) is widely used to improve the disturbance rejection performance [6]. Hence, the simplified ZOH equivalent discrete-time model $G_{p2}(z)$ with ARTF can be derived as follows:

$$\begin{aligned} G_{p2}(z) =& \frac{i_{dq}(z)}{U_{dq}(z)} = \frac{G_{p1}(z)}{\boldsymbol{I}+\boldsymbol{F}G_{p1}(z)} \\ =& \frac{\frac{\boldsymbol{\Delta}}{z(z\boldsymbol{I}-\boldsymbol{\Gamma})}}{\boldsymbol{I}+\frac{\boldsymbol{\Delta}}{z(z\boldsymbol{I}-\Gamma)}} = \frac{\boldsymbol{\Delta}}{z(z\boldsymbol{I}-\boldsymbol{\Gamma})+\boldsymbol{\Xi}} \\ \boldsymbol{\Xi} =& \begin{bmatrix}\frac{R_a}{L_d}T_s & 0\\ 0 & \frac{R_a}{L_q}T_s\end{bmatrix}\boldsymbol{F} = \begin{bmatrix}R_a & 0\\ 0 & R_a\end{bmatrix} \end{aligned} \tag{6}$$

where $\boldsymbol{F}$ is the symmetric matrix of the active resistance $R_a$, i.e., $\boldsymbol{F} = R_a\boldsymbol{I}$. $G_{p2}(z)$ represents the AC machine model with the inner active resistance feedback, which contains the AC machine model transfer function $G_{p1}(z)$ , the transfer function of the feedback path, and the active resistance feedback $\boldsymbol{F}$ .

### B. Deadbeat response current controllers with ARTF

To better elaborate the ARTF structure, three previous digital current controllers with ARTF are illustrated here, namely digital current controller with ARTF by predicted current [17], digital current controller with ARTF by current estimator [18] and IMC digital current controller with ARTF [16].

1) Digital current controller with ARTF by predicted current [17] and digital current controller with ARTF by current estimator [18]: Since the modulation and computation delay can affect the pole-zero cancellation [14], the prediction scheme is adopt herein. These two methods have same structure of AC machines model and controllers, and the latter further employs the predicted current for feedback of the current controller. In addition, the predicted current $z\widehat{i_{dq}}(z)$ is obtained based on AC models in [17] and acquired in proposed current estimator in [18]. In these methods, $G_{p2}(z)$ can be rewritten as:

$$G_{p3}(z) = \frac{i_{dq}(z)}{U_{dq}(z)} = \frac{\boldsymbol{\Delta}}{z(z\boldsymbol{I}-\boldsymbol{\Gamma}+\boldsymbol{\Xi})} \tag{7}$$

The feedback controller $G_{c3}(z)$ can be designed according to pole-zero cancellation as follows:

$$G_{c3}(z) = \alpha\boldsymbol{L}T_s^{-1}e^{2\boldsymbol{J}\omega_e T_s}\left(\boldsymbol{I}-z^{-1}\boldsymbol{\Gamma}+z^{-1}\boldsymbol{\Xi}\right)\frac{z}{z-1} \tag{8}$$

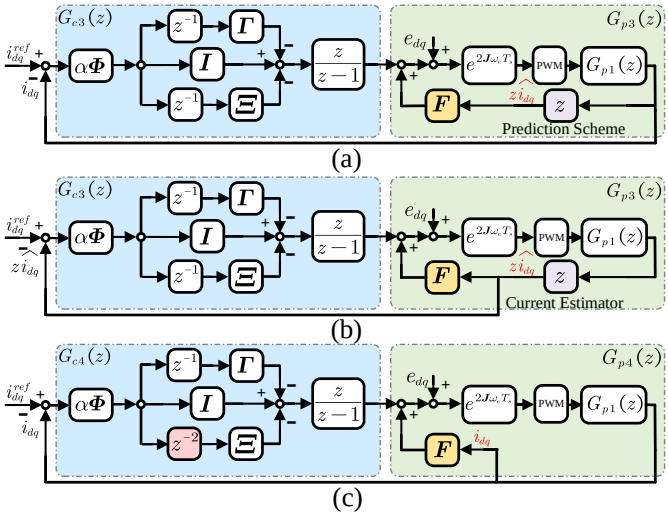


Fig. 1. Block diagrams of three previous digital current controllers with ARTF (a) Digital current controller with ARTF by predicted current. (b) Digital current controller with ARTF by current estimator. (c) IMC digital current controller with ARTF.

where $\alpha$ is the angular frequency of the current controller.

2) IMC digital current controller with ARTF: A delay model is added to suppress the ARTF delay issues [16]. Considering the inherent delay model $z^{-1}$, $G_{p2}(z)$ can be rewritten as:

$$G_{p4}(z)=\frac{i_{dq}(z)}{U_{dq}(z)}=\frac{\boldsymbol{\Delta}}{z\left(z\boldsymbol{I}-\boldsymbol{\Gamma}+z^{-1}\boldsymbol{\Xi}\right)} \tag{9}$$

The internal model control (IMC) method fundamentally involves incorporating the inverse of the plant transfer function (excluding any delays and zeros located in the right-half plane) into the controller structure [4]. In the particular case of current command tracking with PI controllers in AC machines, it is achieved by cancelling the pole of the plant transfer function of the AC machine by a matching zero in the current controller [14]. Hence, according to the pole-zero cancellation, the inherent delay model $z^{-1}$ need to be added into the structure of the current controller [16]. In this way, the current controller should be designed as $G_{p4}^{-1}(z)\,x(z)\,y(z)$ based on the IMC method, where $x(z)$ is an adjustable model based on a plant. In order to build the second-order closed-loop current system transfer function, the discrete-time model $y(z)$ need to be designed as $\frac{z\alpha}{z-1}$ and the $x(z)$ should equal to $z^{-2}$ to make a causal system in the current controller. In this case, the current controller $G_{c4}(z)$ can be presented as follows:

$$G_{c4}(z)=\alpha\boldsymbol{L}T_s^{-1}e^{2\boldsymbol{J}\omega_e T_s}\left(I-z^{-1}\boldsymbol{\Gamma}+z^{-2}\boldsymbol{\Xi}\right)\frac{z}{z-1} \tag{10}$$

The prediction scheme was employed in [17] and [18] to change the plant of AC machines to suppress the ARTF digital delay issue. However, the predictive current control relies heavily on the accuracy of the AC machine parameters [23]. Parameter mismatches can prevent [17] and [18] from correctly altering the plant of the virtual AC machine model, which in turn affects the pole-zero cancellation. In addition, since the feedback path of the active resistance in [17] and [18] is $z\widehat{i_{dq}}(z)\boldsymbol{F}$, where one-step operator $z$ is implemented using the predictive control. Hence, the parameter mismatch

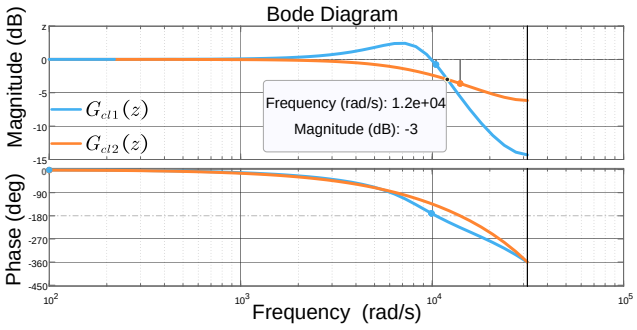


Fig. 2. Block diagrams of dynamic response evaluation (Conditions: $T_s=100\ \mu s$, System bandwidth: $1.2\times10^4\ rad/s$ ).

can also affect the optimum value of active resistance, and the disturbance rejection of the overall system can be affected. In contrast, the method in [16] did not employ the prediction scheme, it only added the inherent delay into the digital current controller. Therefore, compared with the digital current controller with ARTF by prediction scheme, this method can achieve enhanced dynamic response due to better pole-zero cancellation and lower parameter sensitivity. The block diagrams of three above-mentioned digital current controllers are shown in Fig. 1 and $\boldsymbol{\Phi}=\boldsymbol{L}T_s^{-1}$.

3) Proposed deadbeat current controller with ARTF: In the previous method [14], [16], [17], the current controller is designed based on the IMC principle to achieve the pole-zero cancellation and good dynamic response performance [4]. Therefore, the closed-loop current system transfer function $G_{cl1}(z)$ is built as the second-order system:

$$\begin{aligned}G_{cl1}(z)&=\frac{i_{dq}(z)}{i_{dq}^{ref}(z)}=\frac{G_{p4}(z)\,G_{c4}(z)}{1+G_p(z)\,G_{c4}(z)}\\&=\frac{\frac{\alpha T_s}{(z-1)z}}{1+\frac{\alpha T_s}{(z-1)z}}=\frac{\alpha T_s}{z^2-z+\alpha T_s}\end{aligned} \tag{11}$$

However, it can be seen from Fig. 2 and (11) that under the high system bandwidth condition, the closed-loop transfer function between the output current and the reference current $G_{cl1}(z)$ will become the underdamped second-order system, resulting in the current overshoot and oscillations. In [18], the closed-loop current system transfer function $G_{cl2}(z)$ is built as the first-order system since the predicted current is utilized as the ARTF delay compensation and the feedback of the current controller at the same time:

$$\begin{aligned}G_{cl2}(z)=&\frac{i_{dq}(z)}{i_{dq}^{ref}(z)}=\frac{G_{p3}(z)\,G_{c3}(z)}{1+zG_{p3}(z)\,G_{c3}(z)}\\=&\frac{\alpha T_s}{z^2-z+\alpha T_s z}=\frac{\alpha T_s}{z-1+\alpha T_s}\quad\begin{matrix}T_s\ Delay\\ \widehat{\frac{1}{z}}\end{matrix}\end{aligned} \tag{12}$$

It can be seen from (12) and Fig. 2 that the predicted current was employed for the feedback of the current controller, i.e., the gain of the feedback path is the one-step lead operator $z$, the closed-loop transfer function $G_{cl2}(z)$ is changed to the first order system, and there is no current overshoot with the high system bandwidth when the pole is located in the stable

region. The dynamic response is improved and the ARTF delay can be suppressed based on this structure. However, the predictive current control relies heavily on the accuracy of AC machine parameters. Parameter mismatches can affect the accuracy of current prediction, resulting in the closed-loop transfer function that deviates from the desired structure [24]. Besides, the design process of the current estimator is complicated.

Motivated by this fact, since the transfer function of the AC machine model $G_{p2}(z)$ has already known, instead of using the prediction scheme, the proposed current controller $G_{c5}(z)$ can be designed directly based on $G_{cl2}(z)$ as follows:

$$\begin{aligned} G_{cl2}(z) =& \frac{G_{c5}(z) G_{p2}(z)}{1 + G_{c5}(z) G_{p2}(z)} = \frac{\alpha T_s}{z - 1 + \alpha T_s} \cdot \frac{1}{z} \\ G_{c5}(z) =& \frac{\alpha T_s}{(z^2 + z(\alpha T_s - 1) - \alpha T_s) G_{p2}^{-1}(z)} \\ =& \frac{z^2 - z\boldsymbol{\Gamma} + \boldsymbol{\Xi}}{z^2 + \alpha T_s z - z - \alpha T_s} \boldsymbol{L} \alpha e^{2\boldsymbol{J}\omega_e T_s} \end{aligned} \tag{13}$$

In this way, the closed-loop transfer function can still be a first-order system, which can achieve high dynamic response performance while has better parameter robustness performance and easier design process compared to the prediction scheme.

### C. Deadbeat response current controller with high-damped structure

1) Disturbance rejection evaluation of the proposed current controller with ARTF: In order to further investigate the effect of ARTF on the disturbance rejection and current response, the disturbance rejection transfer $G_{d1}(z)$, i.e., the transfer function of the current response $i_{dq}(z)$ produced by the disturbance $D_{dq}(z)$ in the proposed structure can be derived as follows:

$$\begin{aligned} G_{d1}(z) =& \frac{i_{dq}(z)}{D_{dq}(z)} = \frac{G_{p4}(z)}{\boldsymbol{I} + G_{c5}(z) G_{p4}(z)} \\ =& \underbrace{\frac{\boldsymbol{\Delta}\left(z^2 + z(\alpha T_s - 1) - \alpha T_s\right)}{\left(z^2 - z + \alpha T_s z\right)}}_{G_{d\_A}(z)} \underbrace{\frac{}{\left(z^2\boldsymbol{I} - z\boldsymbol{\Gamma} + \boldsymbol{\Xi}\right)}}_{G_{d\_B}(z)} \end{aligned} \tag{14}$$

It can be seen from (14) that $G_{d\_1}(z)$ has two parts of the characteristic polynomial, the poles of $G_{d\_A}(z)$ is consistent with the dynamic response transfer function, and the poles of $G_{d\_B}(z)$ are influenced by active resistance $R_a$. The poles trajectory of $G_{d\_B}(z)$ and step response plot of the disturbance rejection transfer function with varying $R_a$ are shown in Fig. 4. It can be clearly seen that as $R_a$ increases, the poles move towards the region of the low damping and high natural frequencies, and is getting closer to the boundary of the unit circle. The poles with high natural frequency can achieve a quick response to the disturbance to improve the disturbance rejection. However, being close to the boundary of the unit circle will cause low damping ratios and the current oscillation. In addition, the stability of the system will suffer when the value of $R_a$ is too high.

2) High-damped structure design: In order to suppress the negative impact of the ARTF delay on the system and the current response, a compensation term is developed to reconstruct the AC machine model virtually to address these issues. The block diagram of the proposed framework is shown in Fig. 3, where the term $G_{com}(z) = \frac{z}{z+\sigma}$ is added before the ac machine model to rebuilt the system to suppress the digital delay issue caused by the active resistance term feedback. In this way, the transfer function of the discrete-time AC machine model $G_{p5}(z)$ with the compensation term can be derived as follows:

$$\begin{aligned} G_{p5}(z) =& \frac{i_{dq}(z)}{U_{dq}(z)} = \frac{G_{com}(z) G_{p1}(z)}{I + F G_{com}(z) G_{p1}(z)} \\ =& \frac{\frac{z}{z+\sigma}\frac{\boldsymbol{\Delta}}{z(z\boldsymbol{I} - \boldsymbol{\Gamma})}}{I + F\frac{z}{z+\sigma}\frac{\boldsymbol{\Delta}}{z(z\boldsymbol{I} - \boldsymbol{\Gamma})}} = \frac{\frac{\boldsymbol{\Delta}}{(z+\sigma)(z\boldsymbol{I} - \boldsymbol{\Gamma})}}{I + \frac{\boldsymbol{\Xi}}{(z\boldsymbol{I} - \boldsymbol{\Gamma})(z+\sigma)}} \\ =& \frac{\boldsymbol{\Delta}}{(z+\sigma)(z\boldsymbol{I} - \boldsymbol{\Gamma}) + \boldsymbol{\Xi}} \end{aligned} \tag{15}$$

Since the transfer function of the ac machine model with the proposed compensation term $G_{p5}(z)$ in the discrete-time domain has already known, the transfer function of the current controller $G_{c6}(z)$ can be designed based on $G_{cl}(z)$ to achieve the good dynamic response performance:

$$\begin{aligned} G_{cl2}(z) =& \frac{i_{dq}(z)}{i_{dq}^{ref}(z)} = \frac{G_{c6}(z) G_{p5}(z)}{1 + G_{c6}(z) G_{p5}(z)} \\ =& \frac{\alpha T_s}{z - 1 + \alpha T_s} \cdot \frac{1}{z} \\ G_{c6}(z) =& \frac{z^2\boldsymbol{I} + z(\sigma\boldsymbol{I} - \boldsymbol{\Gamma}) - \sigma\boldsymbol{\Gamma} + \boldsymbol{\Xi}}{z^2 + z\alpha T_s - z - \alpha T_s} \boldsymbol{L} \alpha e^{2\boldsymbol{J}\omega_e T_s} \end{aligned} \tag{16}$$

In terms of the disturbance rejection performance evaluation, the disturbance rejection transfer function of the proposed structure $G_{d2}(z)$ can be presented as follows:

$$\begin{aligned} G_{d2}(z) =& \frac{i_{dq}(z)}{D_{dq}(z)} = \frac{G_{p5}(z)}{\boldsymbol{I} + G_{c6}(z) G_{p2}(z)} \\ =& \underbrace{\frac{\boldsymbol{\Delta}\left(z^2 + z(\alpha T_s - 1) z - \alpha T_s\right)}{\left(z^2 - z + z\alpha T_s\right)}}_{G_{d\_C}(z)} \underbrace{\frac{}{\left((z+\sigma)(z\boldsymbol{I} - \boldsymbol{\Gamma}) + \boldsymbol{\Xi}\right)}}_{G_{d\_D}(z)} \end{aligned} \tag{17}$$

It can be seen from (17) that the $G_{d2}(z)$ has the same part $G_{d\_C}(z)$ with $G_{d1}(z)$ which is identical to the dynamic response transfer function, and the poles of $G_{d\_D}(z)$ is influenced by active resistance $R_a$. Fig. 5 depicts the poles migration and the step of the disturbance rejection transfer function with varying $R_a$, and the same system bandwidth and dynamic response performance are set. It can be clearly seen from Fig. 5 (a) that the pole of $G_{d\_D}(z)$ moves towards the center of the unit circle as the active resistance $R_a$ increases within a specific range. Hence, the dynamic response and disturbance rejection are improved simultaneously since the damping ratio and natural angular frequency increase with $R_a$. Therefore, the range of permissible value of $R_a$ is extended without compromising system stability and the oscillation. Moreover, since the compensation term does not require any machine parameter, the proposed current controller can achieve better parameter robustness compared to the digital current controller with ARTF by the prediction scheme.

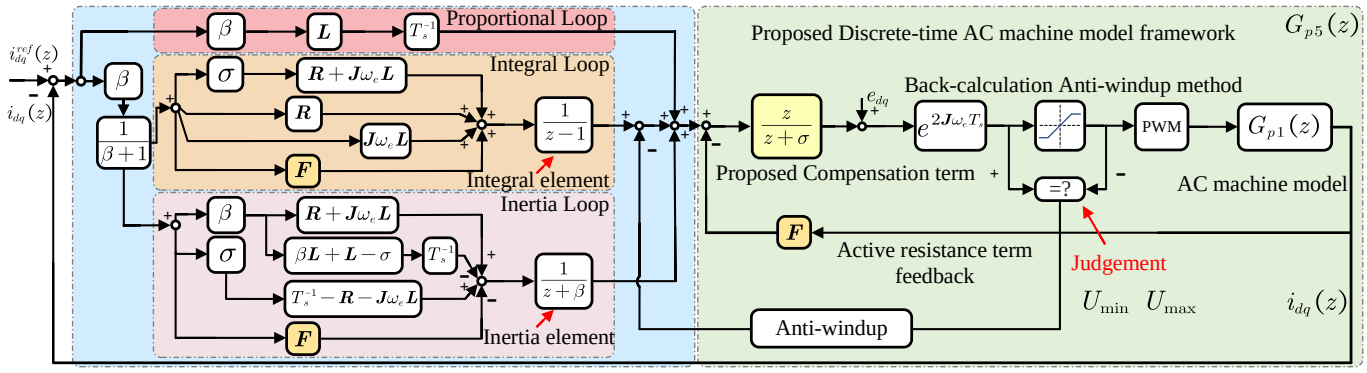


Fig. 3. Block diagram of the proposed current controller.

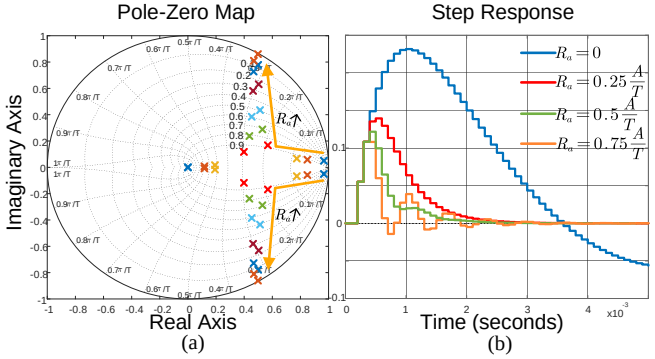


Fig. 4. Simulation plot of disturbance rejection evaluation (Conditions: $T_s = 100\ \mu s$, $\alpha = 0.19$). (a) Poles migration of $G_{d\_B}$ ($R_a$ increases). (b) Step response plot of $G_{d1}(z)$.

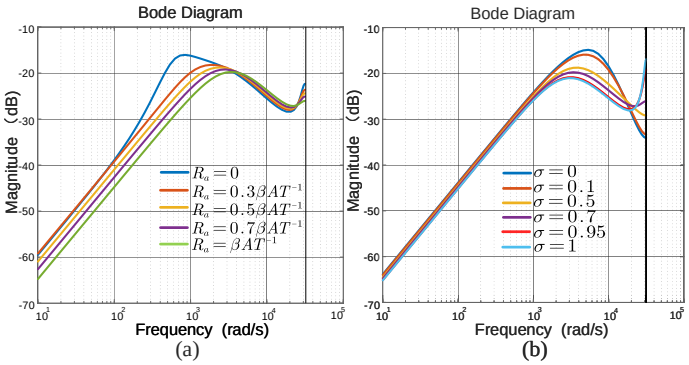


Fig. 6. Simulation plot of disturbance rejection evaluation (Conditions: $T_s = 100\ \mu s$, $\alpha = 0.19$). (a) Bode diagram of $G_{d2}(z)$ with various $R_a$. (b)Bode diagram of $G_{d2}(z)$ with various $\sigma$.

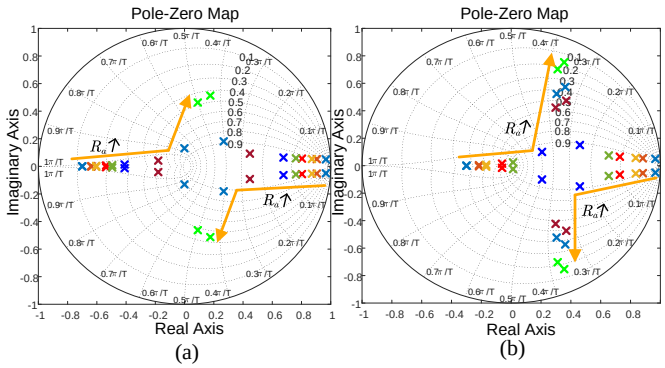


Fig. 5. Simulation plot of disturbance rejection evaluation (Conditions: $T_s = 100\ \mu s$, $\alpha = 0.19$). (a) Poles migration of $G_{d\_D}$ ($R_a$ increase, $\sigma = 0.8$.). (b) Poles migration of $G_{d\_D}$ ($R_a$ increase, $\sigma = 0.2$.).

### *D. Three coefficients design and analysis in the deadbeat response current control framework ( $\beta, R_a, \sigma$)*

1) Dynamic response coefficient: $\beta$. Setting $\beta = \alpha T_s$ to simplify the controller and $\beta$ can be determined by the desired dynamic response performance. In z domain, the system are stable when all poles are located in a unit circle. Hence, $\beta$ need to be satisfied as $\beta \in [0, 1]$. Furthermore, setting $\beta = 1$, the closed-loop transfer function $G_{cl2}(z)$ will become $G_{cl2}(z) = z^{-2}$, and it has the same dynamic characteristic with DPCC [7]. Hence, it can be fully illustrated the proposed digital current controller can achieve the deadbeat response. In addition, the detailed stability criteria with $\beta$ can be referred to [7].

2) Middle frequency disturbance rejection ability coefficient: $R_a$. The increasing of the value of $R_a$ can improve middle-frequency disturbance rejection ability. However, excessive $R_a$ can cause low damping ratios and current oscillations. In this case, the optimal value of $R_a$ can be equal to the proportional gain of the current controller [14], [18]. Therefore, $R_a$ can be set as $\beta A T^{-1}$ in this paper.

3) High frequency disturbance rejection ability coefficient: $\sigma$. It can be seen from Fig. 6 that the high-frequency disturbance rejection ability is influenced by parameter $\sigma$. Based on the stability principle, $\sigma$ need to be satisfied as $\sigma \in [0, 1]$. By comparing Fig. 4 (a) and Fig. 5. (b), it can be seen that the smaller $\sigma$ becomes, the closer the trajectory of the pole of $G_{d\_D}(z)$ moves towards $G_{d\_B}(z)$. It can be seen from Fig. 6 that the increase of the parameter $\sigma$ can suppress the overshoot of the current step response and the current oscillation caused by ARTF, but the high-frequency disturbance rejection ability of the system decreases. Therefore, $\sigma = 0.95$ is considered as the optimal value in this paper. The effect of $\sigma 5$ will be verified in the experiment.

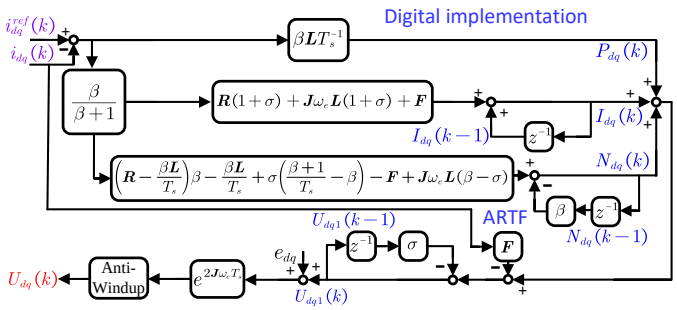


Fig. 7. Digital implementation process of the proposed PIN current controller.

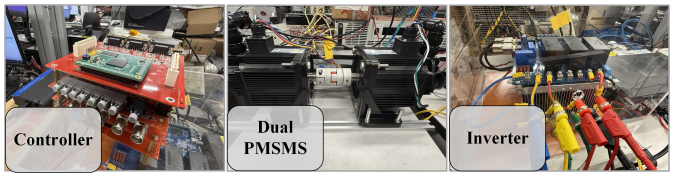


Fig. 8. The experimental platform of the AC machine drive system.

### E. PIN structure digital implementation

Aiming at reducing the computation burden of the digital implementation of the proposed current controller and performing the anti-windup control method, a PIN structure digital implementation is proposed in this paper. The PIN structure can be described by three parts: proportional (P), integral (I) and inertia (N). The transfer function of the proposed current controller $G_{c6}(z)$ can be rewritten as follows:

$$\begin{aligned} G_{c6}(z) =& \frac{\beta \boldsymbol{L}}{T_s} + \frac{\beta}{\beta+1}\left[\boldsymbol{R}(1+\sigma)+\boldsymbol{J}\omega_e\boldsymbol{L}(1+\sigma)+\boldsymbol{F}\right]\frac{1}{z-1} \\ &+ \frac{\beta}{\beta+1}\left[\left(\boldsymbol{R}-\frac{\beta\boldsymbol{L}}{T_s}\right)\beta - \frac{\beta\boldsymbol{L}}{T_s} + \sigma\left(\frac{\beta+1}{T_s}\right) - \boldsymbol{F}\right. \\ &\left. -\sigma\boldsymbol{R}+\boldsymbol{J}\omega_e\boldsymbol{L}(\beta-\sigma)\right]\frac{1}{z+\beta} \end{aligned} \tag{18}$$

Due to the existence of integral term, the back-calculation anti-windup method is adopted [4]. The digital implementation of the proposed PIN current controller is shown in Fig. 7 and the digital kth expression can be presented as follows:

$$\begin{aligned} \delta_{dq}(k) =& i_{dq}^{ref}(k) - i_{dq}(k), P_{dq}(k) = \beta \boldsymbol{L} T_s^{-1}\delta_{dq}(k) \\ I_{dq1}(k) =& \frac{\beta}{\beta+1}\left[\boldsymbol{R}(1+\sigma)+\boldsymbol{J}\omega_e\boldsymbol{A}(1+\sigma)+\boldsymbol{F}\right]\delta_{dq}(k) \\ I_{dq}(k) =& I_{dq1}(k-1) + I_{dq}(k-1) \\ N_{dq1}(k) =& \frac{\beta}{\beta+1}\left[\left(B-\frac{\beta A}{T_s}\right)\beta - \frac{\beta A}{T_s} + \sigma\left(\frac{\beta+1}{T_s}\right)\right. \\ & \left. - F - \sigma\boldsymbol{R}+\boldsymbol{J}\omega_e\boldsymbol{L}(\beta-\sigma)\right]\delta_{dq}(k) \\ N_{dq}(k) =& N_{dq1}(k-1) - \beta N_{dq}(k-1) \\ U_{dq1}(k) =& (P_{dq}(k) + I_{dq}(k) + N_{dq}(k) - \boldsymbol{F} i_{dq}(k)) \\ & - \sigma U_{dq1}(k-1) \\ U_{dq}(k) =& (U_{dq1}(k) + e_{dq}(k))\, e^{2\boldsymbol{J}\omega_e T_s} \end{aligned} \tag{19}$$

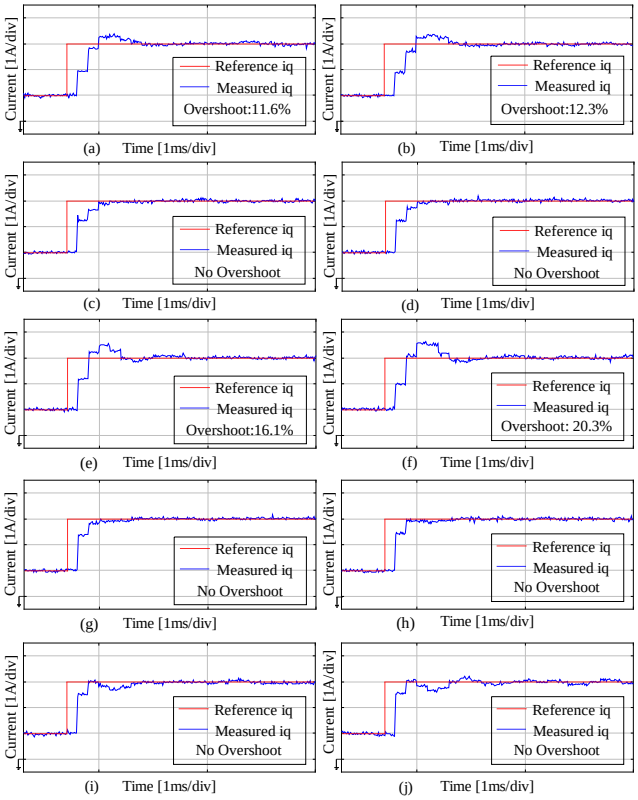


Fig. 9. The current dynamic response of three methods. (a) Method1; (b) Method2; (c) Method3; (d) Method4 with $\sigma = 0.95$; (e) Method1; (f) Method2; (g) Method3; (h) Method4 with $\sigma = 0.95$; (i) Method4 with $\sigma = 0.5$; (j) Method4 with $\sigma = 0.1$.

## IV. Experimental Verification

In order to better validate the properties of the proposed controller (Method4), IMC digital current controller with ARTF [16] (Method1), the digital current controller with ARTF by predicted current [17] (Method2), and the digital current controller with ARTF by the current estimator [18] (Method3) will be compared in this section. The AC machine test platform is shown in Fig. 8. In the platform, two PMSMs are used as drive AC machine and load AC machine, respectively. The inverter is designed based on two level voltage source with silicon carbide modules. The controller DSP (TMS320F28377d) is adopted to execute control algorithms. The sampling time $T_s$ is set as 100 $\mu s$ and the deadtime of the inverter is set as 2.5 $\mu s$. For the AC machine, $L_d = 1.8$ mH, $L_q = 1.8$ mH, and $R_s = 0.6\ \Omega$. In addition, the AC machine has 4 pole pairs with a rotor flux linkage $\psi_f$ of 0.15 Wb.

### A. Dynamic Response Performance Evaluation

Since dynamic performance is very crucial for design of controllers, the dynamic response performance is tested first. Because $\beta$ can determine the system bandwidth (see Fig. 2, point -3 $dB$), i.e., the time when the maximum value of the measured current is approximately 0.707 times of the maximum value of the referenced current [18]. Therefore, in order to obtain the same system bandwidth and make a fair comparison, $\beta = 0.44$ in Method1 and Method2, and $\beta = 0.64$

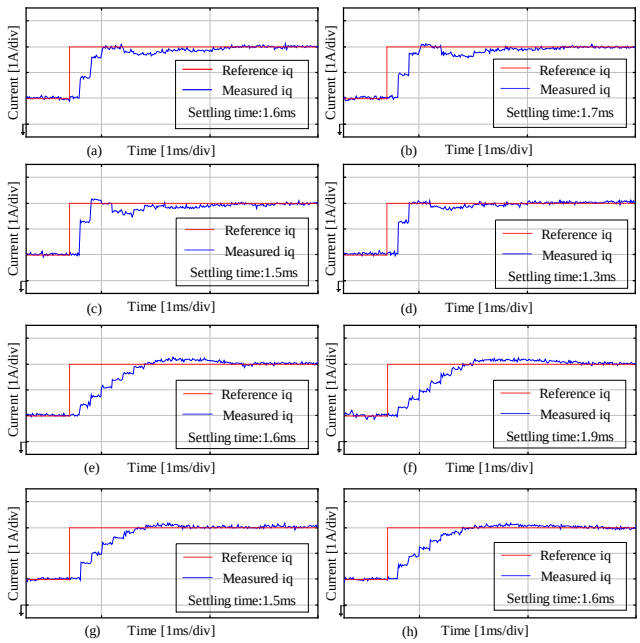


Fig. 10. The current dynamic response of three methods under parameter mismatch. (a) Method1 with $L_{dC} = 1.5L_d$, $L_{qC} = 1.5L_q$; (a) Method2 with $L_{dC} = 1.5L_d$, $L_{qC} = 1.5L_q$; (c) Method3 with $L_{dC} = 1.5L_d$, $L_{qC} = 1.5L_q$; (d) Method4 with $L_{dC} = 1.5L_d$, $L_{qC} = 1.5L_q$; (e) Method1 with $L_{dC} = 0.67L_d$, $L_{qC} = 0.67L_q$; (f) Method2 with $L_{dC} = 0.67L_d$, $L_{qC} = 0.67L_q$; (g) Method3 with $L_{dC} = 0.67L_d$, $L_{qC} = 0.67L_q$; (h) Method4 with $L_{dC} = 0.67L_d$, $L_{qC} = 0.67L_q$.

in Method3 and Method4. In the evaluation, the load machine keeps the constant speed and the q-axis reference current is applied from 1 A to 3 A. It can be seen from Fig. 9 (a) (b) (c) (d) that the four current controllers have the same rising time. However, Method1 and Method2 occur overshoot (11.6 % and 12.3 %, respectively.), and there is no overshoot in Method3 and Method4. When the current bandwidth increases, i.e., $\beta = 0.51$ in Method1 and Method2, and $\beta = 0.67$ in Method3 and Method4. It can be seen that Method 1 and Method 2 show the larger overshoot, but Method3 and the proposed current controller still have no overshoot. Hence, the proposed current controller can achieve good dynamic response performance without employing the prediction scheme.

Furthermore, in order to validate the selection method of the parameter $\sigma$, the experiment of different values of $\sigma$ is carried out. It can be seen from Fig. 9 (i) (j) that although the current has no overshoot, the system occurs the oscillation as $\sigma$ decreases. Hence, the theoretical analysis of Section II.C can be verified, i.e., the poles being close to the boundary of the unit circle will cause system low damping ratios and current oscillations, and $\sigma$ can determine the location of the poles. Therefore, the proposed digital current controller can suppress ARTF delay effect on the system effectively by tuning $\sigma$.

### *B. Parameter Robustness Performance Evaluation*

Due to the magnetic saturation, the inductance mismatch can easily occur during current changes. Hence, the inductance mismatch is carried out first. In addition, in order to make a

TABLE II
CURRENT OVERSHOOT AND SETTLING TIME COMPARISON OF THE FOUR METHODS

| Parameter mismatch condition | Method 1 | Method 2 | Method 3 | Method 4 |
|---|---|---|---|---|
| Settling time under $R_C = 2R_s$ | 1.1 $\mu s$ | 1.2 $\mu s$ | 1 $\mu s$ | 1 $\mu s$ |
| Settling time under $R_C = 0.5R_s$ | 2.1 $\mu s$ | 2.1 $\mu s$ | 2 $\mu s$ | 1.9 $\mu s$ |
| Settling time under $\psi_{fC} = 2\psi_f$ | 2.2 $\mu s$ | 2.7 $\mu s$ | 2.2 $\mu s$ | 2 $\mu s$ |
| Settling time under $\psi_{fC} = 0.5\psi_f$ | 2.3 $\mu s$ | 2 $\mu s$ | 1.8 $\mu s$ | 1.6 $\mu s$ |
| Overshoot under $R_C = 2R_s$ | 0 A | 0 A | 0 A | 0 A |
| Overshoot under $R_C = 0.5R_s$ | 0 A | 0 A | 0 A | 0 A |
| Overshoot under $\psi_{fC} = 2\psi_f$ | 0.11 A | 0.16 A | 0 A | 0 A |
| Overshoot under $\psi_{fC} = 0.5\psi_f$ | 0.18 A | 0.12 A | 0 A | 0 A |

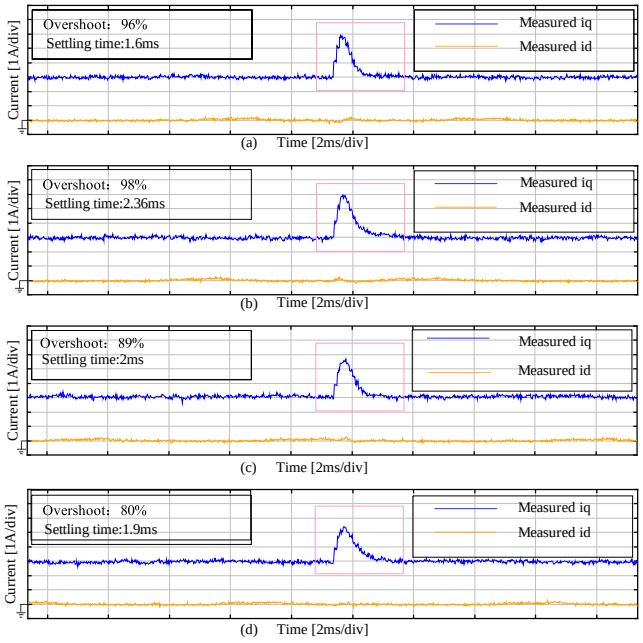


Fig. 11. Disturbance rejection ability performance of three methods. (a) Method1; (b) Method2; (c) Method3; (d) Method4.

fair comparison, the low bandwidth, i.e., $\beta = 0.25$ in Method1 and Method2, and $\beta = 0.37$ in Method3 and Method4 are set to keep the same current dynamic response. It can be seen from Fig. 10 that the inductance mismatch can dramatically affect the current dynamic response performance. In the case of the reduced inductance, all four current controllers occurs the noticeable oscillation. However, the setting time (1.3 $ms$) and amplitude of the oscillation of proposed controller is lower than the Method1 (1.6 $ms$), Method2 (1.7 $ms$) and Method3 (1.5 $ms$). In addition, Method3 occurs the largest overshoot.

In the case of the increased inductance, the dynamic response of the four controllers becomes slower and occurs the overshoot. Although the proposed controller has the same settling time with Method1, the overshoot is much lower than Method1. Furthermore, in order to fully analyze the performance under parameter mismatch in the three methods, the overshoot and settling time of the q-axis current are listed in Table II. From this table, it can be effectively verified that the proposed method is able to suppress the disturbance caused by parameter mismatch and has the best dynamic response performance under parameter mismatch conditions compared

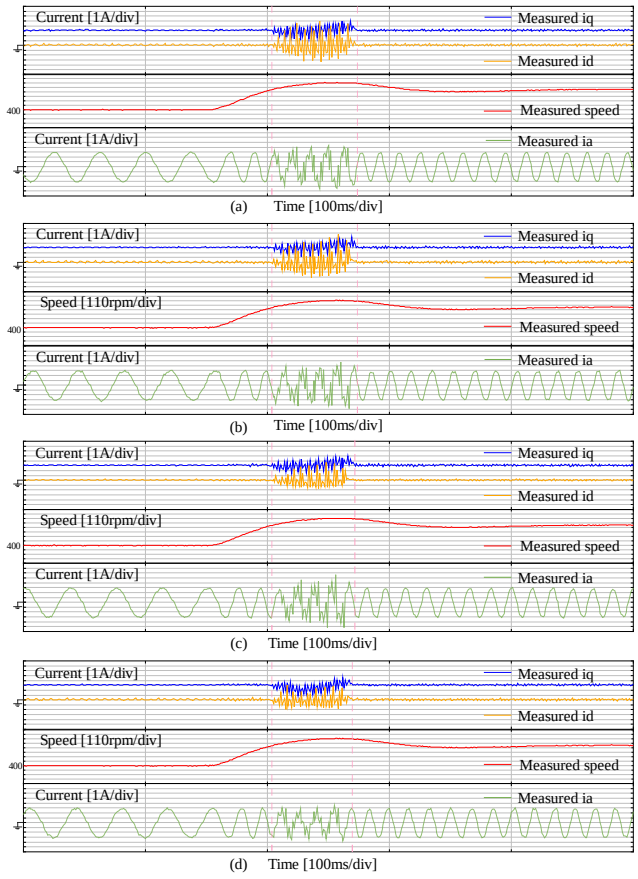


Fig. 12. The steady-state performance with severe parameter mismatch. (a) Method1; (b) Method2; (c) Method3; (d) Method4.

to other methods.

### C. Disturbance Rejection Performance Evaluation

Disturbance rejection ability is a critical factor in evaluating a digital current controller. Hence, the experiment of the external disturbance rejection performance of the three current control methods are carried out in this section. This type of external disturbance is built up by forcing a sudden back EMF change in the current loop feedforward route (see, e.g., [19, Figs. 11], [7, Fig. 15]) and d-axis current can only be affected lightly due to the dq-axis coupling mechanism. The dq-axis reference currents are set to 0 A and 2 A, respectively, and the load machine keeps 400 rpm speed. In addition, the same system bandwidth and dynamic response performance are set in three current control methods to make a fair comparison. It can be seen from Fig. 11 that although the Method1 has the shortest settling time (1.6 $ms$) compared to other methods (2.36 $ms$ in Method2, 2 $ms$ in Method3 and 1.9 $ms$ in Method4), the overshoot in Method4 (80 $\%$) is much lower than Method1 (96 $\%$) and Method2 (98 $\%$), and Method3 (89 $\%$). Therefore, it can be validated that the proposed current control method is able to suppress the external disturbance effectively.

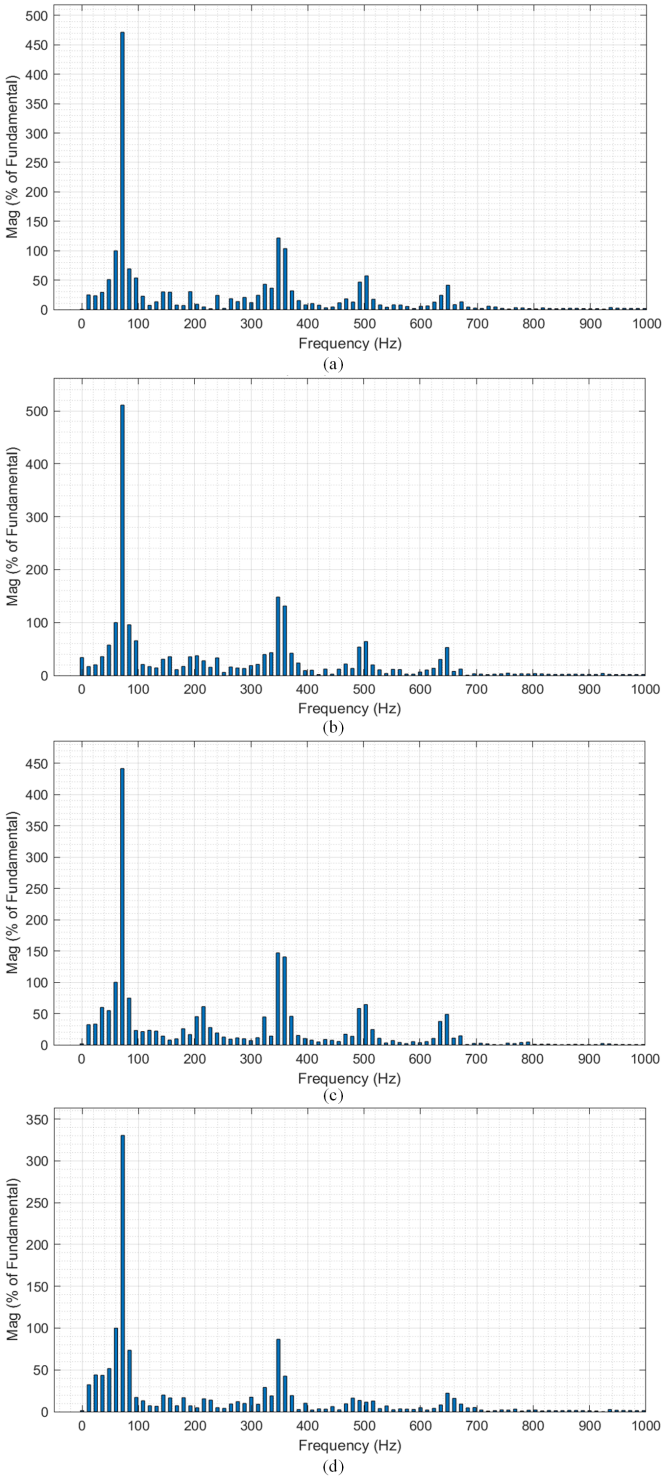


Fig. 13. Frequency domain analysis of the current oscillation. (a) Method1; (b) Method2; (c) Method3; (d) Method4.

### D. Steady-State Performance Evaluation Under Variable Speed Condition

Aiming at testing the steady-state performance under variable speed condition and further verifying the parameter robustness of the proposed controller, the drive machine works under severe parameter mismatch condition, i.e., $L_{dC} =$

TABLE III
COMPUTATION TIME OF THE FOUR CURRENT CONTROL METHODS

| | Method 1 | Method 2 | Method 3 | Method 4 |
|---|---|---|---|---|
| Computation time | 8.56 $\mu s$ | 11.2 $\mu s$ | 12.1 $\mu s$ | 6.72 $\mu s$ |

$1.5L_d$, $L_{qC} = 1.5L_q$, $R_C = 2R_s$, $\psi_C = 1.5\psi_f$, and setting the dq-axis reference current to 0 A and 3 A, respectively.The speed of the load machine is increased from 400 rpm to 900 rpm suddenly, and the system bandwidth in three methods keeps same to make a fair comparison. In addition, it should be noted that the magnitudes of disturbance is further increased due to the flux linkage mismatch. It can be observed from Fig. 12 that all four current control methods can keep the system stability. However, all four current control methods occur the current oscillations and dq-axis cross-coupling phenomenon due to the inductance mismatch [4]. It can be seen that Method1 has the similar settling time and magnitudes of oscillation compared to Method2. The regulation time of Method3 is similar to that of Methods1 and Method2, but the oscillation amplitude of Method3 is reduced. Method4 has the shortest settling time and occurs the minimal oscillation compared to other methods. The frequency-domain analysis of the current oscillation is depicted in Fig.13. The proposed controller can maintain the current more effectively and exhibits lower overshoot during oscillations. As a result, the amplitude of the fundamental frequency in the frequency spectrum is significantly lower than that of other current controllers. Furthermore, it can be seen that the high-frequency components of the oscillating current in the proposed current controller are reduced compared to other current controllers.

### *E. Computational Burden Evaluation*

For the digital current controller, it is essential to know the computation time of the control algorithm. Table III shows the computation time of three control methods. It can be seen that the computation time of the proposed method is 6.72 $\mu s$, which is shorter than other methods (8.56 $\mu s$ in Method1, 11.2 $\mu s$ in Method2, and 12.1 $\mu s$ in Method3). In addition, since the system control period is set to 100 $\mu s$ in the experiment, the computational time of the proposed method only occupies no more than 0.07 of the control period. Therefore, it can be fully validated that the proposed method has low computational burden and can be utilized in practice.

## V. Conclusion

In this paper, a novel framework of digital current controller based on ARTF structure is proposed to solve the issues that the complexity of the exact discrete-time AC machine model, the performance degradation of the PI controller at the high bandwidth, and the ARTF delay effect on the current response. First, the control delay caused by the digital system and the ARTF delay effect on the system are analyzed in detail. Meanwhile, the parameter tuning method and simplification of the proposed controller are carried out theoretically. Finally, the proposed current controller are verified on the dual AC machine platform. The experimental results shows that the proposed digital current controller can reduce the current overshoot and settling time, possess best disturbance rejection ability and parameter robustness performance compared to other methods. Furthermore, the proposed controller has the lower computational burden than other methods. Hence, the proposed digital current controller can be implemented in high performance and high power applications.

The future perspective for this work can be listed as follows. The conjugate poles introduced by ARTF can cause the oscillation response, the new framework will be investigated to eliminate this oscillation problem completely. Advanced modulation and sampling techniques should be developed to further suppress the digital delay.

## References


[1] X. Sun, M. Wu, G. Lei, Y. Guo, and J. Zhu, "An improved model predictive current control for pmsm drives based on current track circle," *IEEE Transactions on Industrial Electronics*, vol. 68, DOI 10.1109/TIE.2020.2984433, no. 5, pp. 3782–3793, 2021.

[2] X. Zhang, B. Hou, and Y. Mei, "Deadbeat predictive current control of permanent-magnet synchronous motors with stator current and disturbance observer," *IEEE Transactions on Power Electronics*, vol. 32, DOI 10.1109/TPEL.2016.2592534, no. 5, pp. 3818–3834, 2017.

[3] Y. Wang, W. Liao, S. Huang, J. Zhang, M. Yang, C. Li, and S. Huang, "A robust dpcc for ipmsm based on a full parameter identification method," *IEEE Transactions on Industrial Electronics*, vol. 70, DOI 10.1109/TIE.2022.3212371, no. 8, pp. 7695–7705, 2023.

[4] L. Harnefors and H.-P. Nee, "Model-based current control of ac machines using the internal model control method," *IEEE Transactions on Industry Applications*, vol. 34, DOI 10.1109/28.658735, no. 1, pp. 133–141, 1998.

[5] F. del Blanco, M. Degner, and R. Lorenz, "Dynamic analysis of current regulators for ac motors using complex vectors," *IEEE Transactions on Industry Applications*, vol. 35, DOI 10.1109/28.806058, no. 6, pp. 1424–1432, 1999.

[6] F. Briz, M. Degner, and R. Lorenz, "Analysis and design of current regulators using complex vectors," *IEEE Transactions on Industry Applications*, vol. 36, DOI 10.1109/28.845057, no. 3, pp. 817–825, 2000.

[7] X. Yuan and C. H. T. Lee, "A simple three-degree-of-freedom digital current controller with dead beat response for ac machines," *IEEE Transactions on Industrial Electronics*, vol. 69, DOI 10.1109/TIE.2021.3109540, no. 8, pp. 7848–7858, 2022.

[8] J. Wen, X. Yuan, S. Niu, and W. L. Chan, "A robust complex vector pi current controller with deadbeat response for pmsm drives," *IEEE Transactions on Industrial Electronics*, DOI 10.1109/TIE.2024.3482013, pp. 1–11, 2024.

[9] T. Turker, U. Buyukkeles, and A. F. Bakan, "A robust predictive current controller for pmsm drives," *IEEE Transactions on Industrial Electronics*, vol. 63, DOI 10.1109/TIE.2016.2521338, no. 6, pp. 3906–3914, 2016.

[10] H. Kim, M. W. Degner, J. M. Guerrero, F. Briz, and R. D. Lorenz, "Discrete-time current regulator design for ac machine drives," *IEEE Transactions on Industry Applications*, vol. 46, DOI 10.1109/TIA.2010.2049628, no. 4, pp. 1425–1435, 2010.

[11] M. Hinkkanen, H. Asad Ali Awan, Z. Qu, T. Tuovinen, and F. Briz, "Current control for synchronous motor drives: Direct discrete-time pole-placement design," *IEEE Transactions on Industry Applications*, vol. 52, DOI 10.1109/TIA.2015.2495288, no. 2, pp. 1530–1541, 2016.

[12] M. Hu, W. Hua, Z. Wu, and Y. Hu, "Discrete-time current control of salient machines with a simplified model," *IEEE Transactions on Industrial Electronics*, vol. 70, DOI 10.1109/TIE.2022.3199858, no. 7, pp. 6686–6698, 2023.

[13] H. Kim and R. Lorenz, "Synchronous frame pi current regulators in a virtually translated system," in *Conference Record of the 2004 IEEE Industry Applications Conference, 2004. 39th IAS Annual Meeting.*, vol. 2, DOI 10.1109/IAS.2004.1348513, pp. 856–863 vol.2, 2004.

[14] A. G. Yepes, A. Vidal, J. Malvar, O. Lopez, and J. Doval-Gandoy, "Tuning method aimed at optimized settling time and overshoot for synchronous proportional-integral current control in electric machines," *IEEE Transactions on Power Electronics*, vol. 29, DOI 10.1109/TPEL.2013.2276059, no. 6, pp. 3041–3054, 2014.
[15] S. Zhu, W. Huang, Y. Yan, and Z. Niu, "High-damped complex vector current regulator for pmsm based on active damping function," *IEEE Transactions on Power Electronics*, vol. 38, DOI 10.1109/TPEL.2022.3230350, no. 4, pp. 5204–5216, 2023.
[16] S. N. Vukosavic, L. S. Peric, and E. Levi, "Digital current controller with error-free feedback acquisition and active resistance," *IEEE Transactions on Industrial Electronics*, vol. 65, DOI 10.1109/TIE.2017.2745476, no. 3, pp. 1980–1990, 2018.
[17] J.-S. Yim, S.-K. Sul, B.-H. Bae, N. R. Patel, and S. Hiti, "Modified current control schemes for high-performance permanent-magnet ac drives with low sampling to operating frequency ratio," *IEEE Transactions on Industry Applications*, vol. 45, DOI 10.1109/TIA.2009.2013600, no. 2, pp. 763–771, 2009.
[18] X. Yuan, J. Mei, J. Chen, Y. Zuo, and C. H. T. Lee, "A digital current controller based on active resistance term feedback for spmsm drives," *IEEE Transactions on Power Electronics*, vol. 37, DOI 10.1109/TPEL.2022.3153057, no. 8, pp. 9827–9839, 2022.
[19] X. Yuan, Y. Zuo, Y. Fan, and C. H. T. Lee, "Model-free predictive current control of spmsm drives using extended state observer," *IEEE Transactions on Industrial Electronics*, vol. 69, DOI 10.1109/TIE.2021.3095816, no. 7, pp. 6540–6550, 2022.
[20] J.-W. Choi and S.-K. Sul, "Inverter output voltage synthesis using novel dead time compensation," *IEEE Transactions on Power Electronics*, vol. 11, DOI 10.1109/63.486169, no. 2, pp. 221–227, 1996.
[21] A. Cichowski and J. Nieznanski, "Self-tuning dead-time compensation method for voltage-source inverters," *IEEE Power Electronics Letters*, vol. 3, DOI 10.1109/LPEL.2005.851310, no. 2, pp. 72–75, 2005.
[22] G. Pellegrino, R. I. Bojoi, P. Guglielmi, and F. Cupertino, "Accurate inverter error compensation and related self-commissioning scheme in sensorless induction motor drives," *IEEE Transactions on Industry Applications*, vol. 46, DOI 10.1109/TIA.2010.2057395, no. 5, pp. 1970–1978, 2010.
[23] Y. Zhang, J. Jin, and L. Huang, "Model-free predictive current control of pmsm drives based on extended state observer using ultralocal model," *IEEE Transactions on Industrial Electronics*, vol. 68, DOI 10.1109/TIE.2020.2970660, no. 2, pp. 993–1003, 2021.
[24] X. Zhang and Y. Cao, "A simple deadbeat predictive current control for pmsm with parameter robustness improvement," *IEEE Journal of Emerging and Selected Topics in Power Electronics*, vol. 13, DOI 10.1109/JESTPE.2024.3525140, no. 1, pp. 759–770, 2025.

**Xin Yuan** (Senior Member, IEEE) received the B.Sc. degree in electrical engineering and automation from Beijing Union University, Beijing, China, in 2013, the M.Phil. degree from the North China University of Technology, Beijing, in 2016, and the Ph.D. degree from Beijing Institute of Technology, Beijing, in 2020, both in electrical engineering.

He joined the School of Engineering with the University of Aberdeen, Aberdeen, U.K. as a Lecturer (Assistant Professor), in 2024. Before joining the University of Aberdeen, he worked as a Research Assistant Professor with the Department of Electrical and Electronic Engineering, The Hong Kong Polytechnic University, Hong Kong, China and as a Research Associate with the PEMC Group, University of Nottingham, Nottingham, U.K. In 2020, he was also a Postdoctoral Research Fellow with the School of Electrical and Electronic Engineering, Nanyang Technological University, Singapore.

**Junkai Wen** received the B.Eng. degree in electrical engineering and automation from the Shanghai Ocean University, Shanghai, China, in 2021, and the M.Sc. degree in electrical power system with Distinction from University of Birmingham in 2022. He is currently working toward the Ph,D. degree in Department of Electrical and Electronic Engineering, The Hong Kong Polytechnic University, Hong Kong, China.

His research interests include AC motor drives and power electronics.

**Shuangxia Niu** (Senior Member, IEEE) received the B.Sc. and M.Sc. degrees from Tianjin University, Tianjin, China, in 2002 and 2005, and the Ph.D. degree from the University of Hong Kong, Hong Kong, SAR, China, in 2009, all in electrical engineering.

She is currently a professor with the Department of Electrical and Electronic Engineering, The Hong Kong Polytechnic University. She authored or coauthored more than 200 papers in leading journals.

Prof. Niu is currently an Associate Editor for the IEEE Transactions on Industrial Electronics and the IEEE Journal of Emerging and Selected Topics in Power Electronics. She is Distinguish Lecturer of IEEE Vehicular Technology Society.

**Mingjin Hu** (S'20) was born in Jiangxi, China, in 1994. He received the B.S. and Ph.D. degrees in electrical engineering from the School of Electrical Engineering, Southeast University, Nanjing, China, in 2016 and 2023, respectively. He is currently a Postdoctoral Research Fellow with the Department of Electrical and Electronic Engineering, Hong Kong Polytechnic University.

His research interests include PMSM systems, multiphase motor drives and digital control techniques.